Pacific and Atlantic multidecadal variability in the Kiel Climate Model

Wonsun Park[1] and Mojib Latif[1]

Received 20 September 2010; revised 8 November 2010; accepted 12 November 2010; published 17 December 2010.

[1] Pacific decadal variability (PDV) and Atlantic multidecadal variability (AMV), the two leading decadal modes of observed Northern Hemisphere sea surface temperature (SST) variability, are investigated in a multi-millennial control integration of the Kiel Climate Model (KCM). It is shown that the two phenomena are independent modes in the model and can be easily separated by Principal Oscillation Pattern (POP) analysis of model SST. PDV-related variability covers the whole North Pacific with strong signals in both the mid-latitude North Pacific and the western Tropical Pacific. Strong signals are also simulated in the eastern Indian Ocean Sector. PDV's memory, however, resides in the North Pacific and is linked to the subtropical gyre. The AMV mechanism is related to the Atlantic meridional overturning circulation (AMOC). A stochastic mechanism applies to both PDV and AMV. **Citation:** Park, W., and M. Latif (2010), Pacific and Atlantic multidecadal variability in the Kiel Climate Model, *Geophys. Res. Lett.*, *37*, L24702, doi:10.1029/2010GL045560.

1. Introduction

[2] Climate exhibits a wide range of variability from seasonal to millennial timescales, which has been established from modern observations and paleo-reconstructions. Decadal and multidecadal timescale variability is of particular importance in the context of anthropogenic climate change, as it has the potential to mask the latter and hinder its early detection. In the North Atlantic, multidecadal variability, known as Atlantic multidecadal variability (AMV), has been reported, for instance, by *Delworth et al.* [1993], *Kushnir* [1994] and *Goldenberg et al.* [2001]. AMV is related to AMOC variations in many climate models [e.g., *Delworth et al.*, 1993; *Timmermann et al.*, 1998; *Knight et al.*, 2005; *Zhang and Delworth*, 2006]. Due to the strong involvement of ocean dynamics in the models decadal predictability over the North Atlantic is believed to be relatively high [e.g., *Latif et al.*, 2006]. In the North Pacific, the Pacific Decadal Oscillation (PDO) [e.g., *Mantua et al.*, 1997] is the dominant mode of variability and referred to as the Pacific decadal variability (PDV) here. Both mechanisms internal to the North Pacific [e.g., *Latif and Barnett*, 1994; *Liu et al.*, 2002] and remote forcing from the Tropical Pacific [e.g., *Trenberth and Hurrell*, 1994; *Gu and Philander*, 1997] have been proposed to explain PDV.

[3] It is still not clear whether PDV and AMV are independent modes or related in some way. *d'Orgeville and Peltier* [2007] analyzing observed sea surface temperature (SST) reported that the multidecadal component of the PDO (here PDV) is strongly time-lag correlated with the AMO (here AMV). *Zhang and Delworth* [2007] investigating hybrid coupled model results found that the AMO can contribute to PDO. Observational data are rather short and cover only the period from about 1900 onwards. This is not sufficient to deal with these long timescales in a statistically meaningful way. The study of *Zhang and Delworth* [2007] is limited with respect to studying the link between AMV and PDV, as SST changes are in principle prescribed from observations in the Atlantic basin of their model. Here we use a multi-millennial control integration of KCM to address the connection between PDV and AMV. The run is relatively long, which allows the assessment of statistical significance, and retains full coupling globally. Additionally, we briefly investigate the mechanisms underlying PDV and AMV.

2. Model and Statistical Method

[4] The Kiel Climate Model (KCM) described in detail by *Park et al.* [2009] consists of the ECHAM5 [*Roeckner et al.*, 2003] atmosphere general circulation model coupled to the NEMO [*Madec*, 2008] ocean-sea ice general circulation model, with the OASIS3 coupler [*Valcke*, 2006]. No form of flux correction or anomaly coupling is used. The atmospheric resolution is T31 (3.75° × 3.75°) horizontally with 19 vertical levels. The horizontal ocean resolution is based on a 2° Mercator mesh and is on average 1.3°, with enhanced meridional resolution of 0.5° in the equatorial region and with 31 levels in the vertical. KCM simulates tropical Pacific climate reasonably well compared to observations in terms of its annual cycle and interannual variability [*Park et al.*, 2009]. *Park and Latif* [2008] present the meridional overturning circulation in the Atlantic (AMOC) and its variability at multidecadal and multicentennial timescales in a multi-millennial control simulation. KCM employs rather coarse horizontal resolution, and this may influence the results. It is known, for instance, that the atmospheric response to mid-latitudinal SST anomalies near fronts dramatically changes with enhanced horizontal resolution [e.g., *Minobe et al.*, 2008]. Although desirable, higher resolution would require much more computer resources inhibiting integration times of millennia.

[5] Here, we use 1000 years from the simulation described above and apply Principal Oscillation Pattern (POP) analysis [*Hasselmann*, 1988; *Von Storch et al.*, 1988] to Northern Hemisphere (20°–70°N, 120°–20°E) SST. In contrast to Empirical Orthogonal Function (EOF) analysis

[1]Leibniz-Institut für Meereswissenschaften an der Universität Kiel (IFM-GEOMAR), Kiel, Germany.

0094-8276/10/2010GL045560

that considers only the spatial co-variability in a dataset, the POP method considers the full space-time structure. POPs are in general complex with real part (P_{Real}) and imaginary part (P_{Imag}). The corresponding complex coefficient time series (PCs) satisfy the standard damped harmonic oscillator equation, so that the evolution of the system in the two-dimensional POP space spanned by the real and imaginary part can be interpreted as a cyclic sequence of spatial patterns

$$\ldots \rightarrow P_{Real} \rightarrow -P_{Imag} \rightarrow -P_{Real} \rightarrow P_{Imag} \rightarrow P_{Real} \rightarrow \ldots \quad (1)$$

Complex POPs describe oscillatory modes, propagating or stationary. The characteristic period to complete a full cycle is referred to as rotation period and the e-folding time for exponential decay as damping time. Band-pass filtering was applied (retaining all variability in the range 30–90 years) to highlight the multidecadal variability which is the focus of this study, and annual SST anomalies (calculated by removing the long-term mean) computed. Finally, an EOF analysis of the filtered data was performed, and only the leading ten EOF modes explaining about 88% of the variance were retained in the POP analysis. We note that the SST data were area-weighted prior to the analysis and no normalization was applied.

3. Results

[6] The leading POP mode (Figures 1a–1c) accounting for about 42% of the (filtered) variability is oscillatory and represents the model's PDV. It is associated with an oscillation period of about 46 years and a damping time of about 175 years. Strong loadings are only found in the Pacific, indicating that this mode is internal to the Pacific. Its real part (Figure 1a) represents the well-known PDO-like pattern with strong SST anomalies centered in the western and central North Pacific (Figure 1a) which are surrounded by SST anomalies of opposite sign. The imaginary part (Figures 1b) exhibits only weak loadings, so that the POP mode can be regarded to first order as stationary in SST. However, a weak anti-cyclonic rotation around the subtropical gyre can be inferred from the two POP patterns.

[7] The second most energetic POP mode (Figures 1d–1f) accounting for about 20% of the (filtered) variability is also oscillatory and characterized by a period of 60 years and damping time of 144 years. This mode exhibits strong loadings basically only in the Atlantic and is the model's version of the AMV. The real and imaginary part PCs (Figures 1c and 1f) show, as theoretically expected, a phase shift of about 90 degrees during most of the analyzed period for both modes, which together with the relatively long damping times indicates that the two POPs are indeed oscillatory in nature.

[8] The real part pattern of POP2 (Figure 1d) displays positive SST anomalies which cover most of the North Atlantic, similar to what has been reported from observed multidecadal variability [e.g., *Kushnir*, 1994; *Knight et al.*, 2005]. Details of the real part pattern, however, display noticeable differences to observations. The imaginary part (Figure 1e) also exhibits strong loadings with a tripolar SST anomaly structure in the North Atlantic, indicating, in contrast to PDV, non-stationary behavior in AMV-related SST variability. The second POP mode can be identified with the multidecadal AMOC mode that has been previously described by *Park and Latif* [2008].

[9] The PDV and AMV POP are orthogonal, as can be inferred from the cumulative explained variance, which amounts to the sum of the two individual explained variances. POPs, by definition, are not necessarily orthogonal, which is different from EOFs. However, the two modes are orthogonal in the present analysis so that they indeed represent independent modes with different underlying dynamical processes. Furthermore, no statistically significant correlation is found at any lag between the time series of the two POP modes. We also computed the lag-correlation between the traditional PDO and AMO indices and did not find a statistically significant link. Finally, the POP period of PDV and AMV, although both multidecadal, are different. A major result of this study is thus that PDV and AMV are independent phenomena in KCM.

3.1. Pacific Decadal Variability

[10] We next investigate the regression patterns (maps of local regression coefficients) of selected atmospheric and oceanic variables onto the PCs of POP1 (Figure 2). Figure 2 (left) show the regressions with respect to the real part PC. The surface air temperature (SAT) anomaly pattern (Figure 2a) features a strong connection between the tropical and extratropical Pacific. Overall it looks El Niño/Southern Oscillation (ENSO)-like with positive anomalies over the Equatorial Pacific, negative anomalies in the mid-latitude North Pacific, positive anomalies over northern North America, and negative SAT anomalies over the southeastern United States. Anomalously low SLP is simulated over most of the North Pacific (Figure 2c) and anomalously high pressure over the Indian Ocean. Strong precipitation anomalies are simulated in the Tropics, with strongly reduced rainfall over the Equatorial Indian Ocean and anomalously strong rainfall over the western Equatorial Pacific (Figure 2e). Such connections between the Tropics and the North Pacific were described from the instrumental record [*Deser et al.*, 2004] and from paleo-reconstructions [*D'Arrigo et al.*, 2005]. Enhanced rainfall is also simulated over the mid-latitude North Pacific which extends to western North America. The sea surface height (SSH) anomaly pattern (Figure 2g) serves here as a measure of upper ocean heat content. Strong signals are found north of the Equator in the Pacific with positive anomalies centered at about 10°N and negative anomalies at about 40°N. These SSH changes appear to be entirely consistent with the corresponding wind stress changes (Figure 2c). Anomalous westerlies centered in the region 30°–40°N and anomalous easterlies to the north in the region 50°–60°N both associated with the deepening of pressure over the North Pacific lead to characteristic wind stress curl changes which force an intensification of both the subtropical and the subtropical gyre.

[11] The imaginary part PC regression patterns are shown in Figure 2 (right). Anomalies are generally much weaker compared to the real part patterns, suggesting stationary behavior for most variables. The only exception is the SSH anomaly pattern which displays anomalies that explain a relatively large amount of variance and similar features to those described by *Latif and Barnett* [1994] with a clockwise rotation of the anomalies around the subtropical gyre. This suggests that processes associated with the subtropical gyre provide the memory for the PDV, and that remote

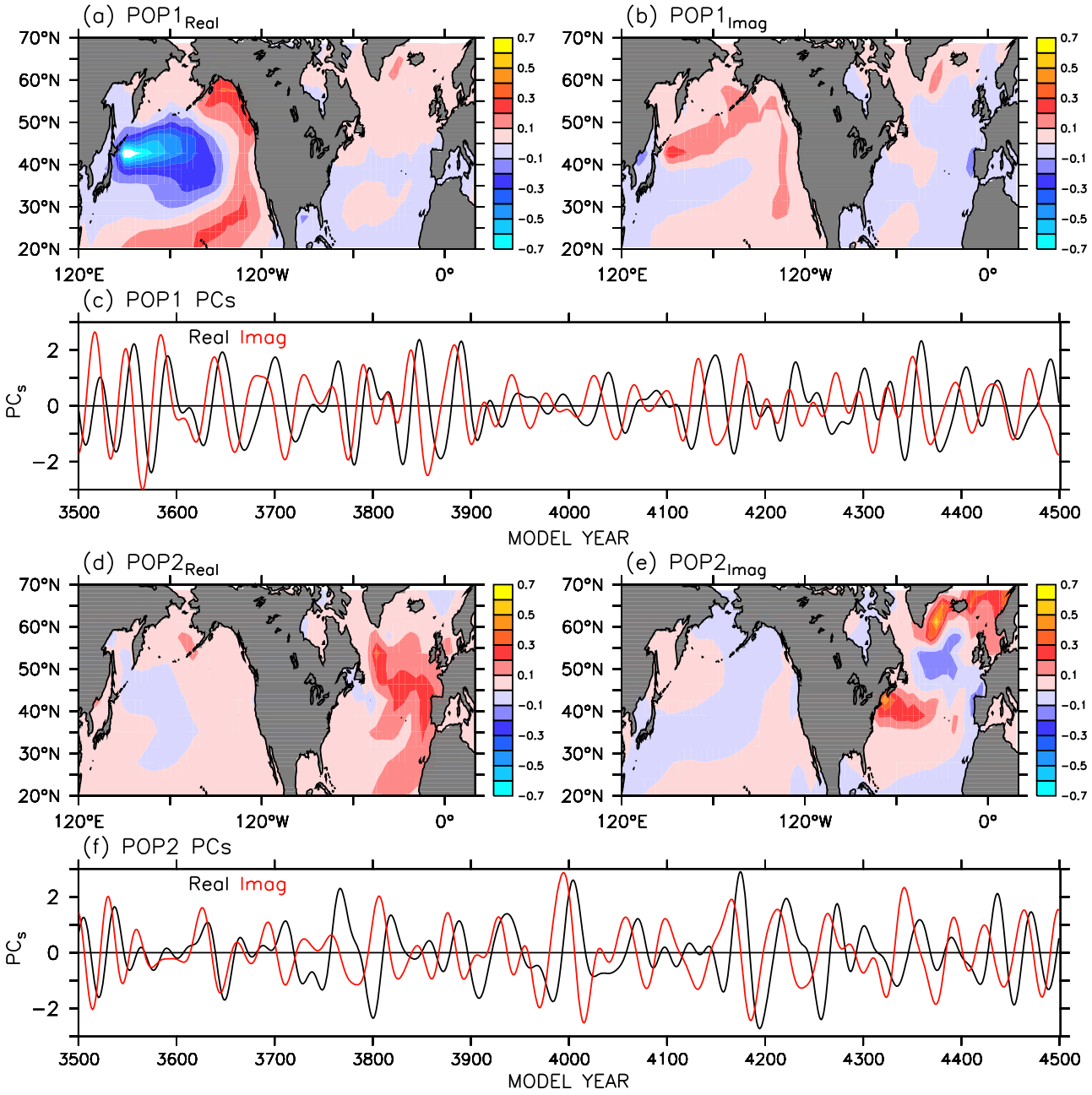

Figure 1. The two leading POP modes of band-pass (30–90 years) filtered annual SST anomalies over the North Pacific and North Atlantic Oceans. The first and second POPs represent 42% and 20% of the filtered variability, respectively. (a) Real part pattern of POP1, (b) imaginary part pattern of POP1, (c) their corresponding PCs, (d) real part pattern of POP2, (e) imaginary part pattern of POP2, and (f) their corresponding PCs. The patterns are in units of [°C]. The PC time series are in units of standard deviations.

forcing from the Equatorial Pacific is of less importance in generating PDV in the model. A hyper mode mechanism may explain the strong tropical signals at these long timescales, as suggested by *Dommenget and Latif* [2008]. This is supported by the location of the SST anomalies in the western Pacific/ Indian Ocean Sector. We computed spectra of North Pacific SLP anomalies and found them to be white to first order. This suggests a stochastic mechanism similar to that proposed by *Latif* [2006]. Further analysis, however, is needed to describe the complete mechanism.

3.2. North Atlantic Variability

[12] We turn now to the AMV as given by the second most energetic POP mode. Exactly the same regression analysis as that described above was performed (Figure 3). The imaginary part regression patterns are shown in Figure 3 (right). The SAT anomaly pattern (Figure 3b) is characterized by a tripolar structure in the North Atlantic with strong positive SAT anomalies explaining more than 20% of the variance in the filtered data in the Greenland-Iceland-Norwegian (GIN) Sea, anomalously cold SST to the south,

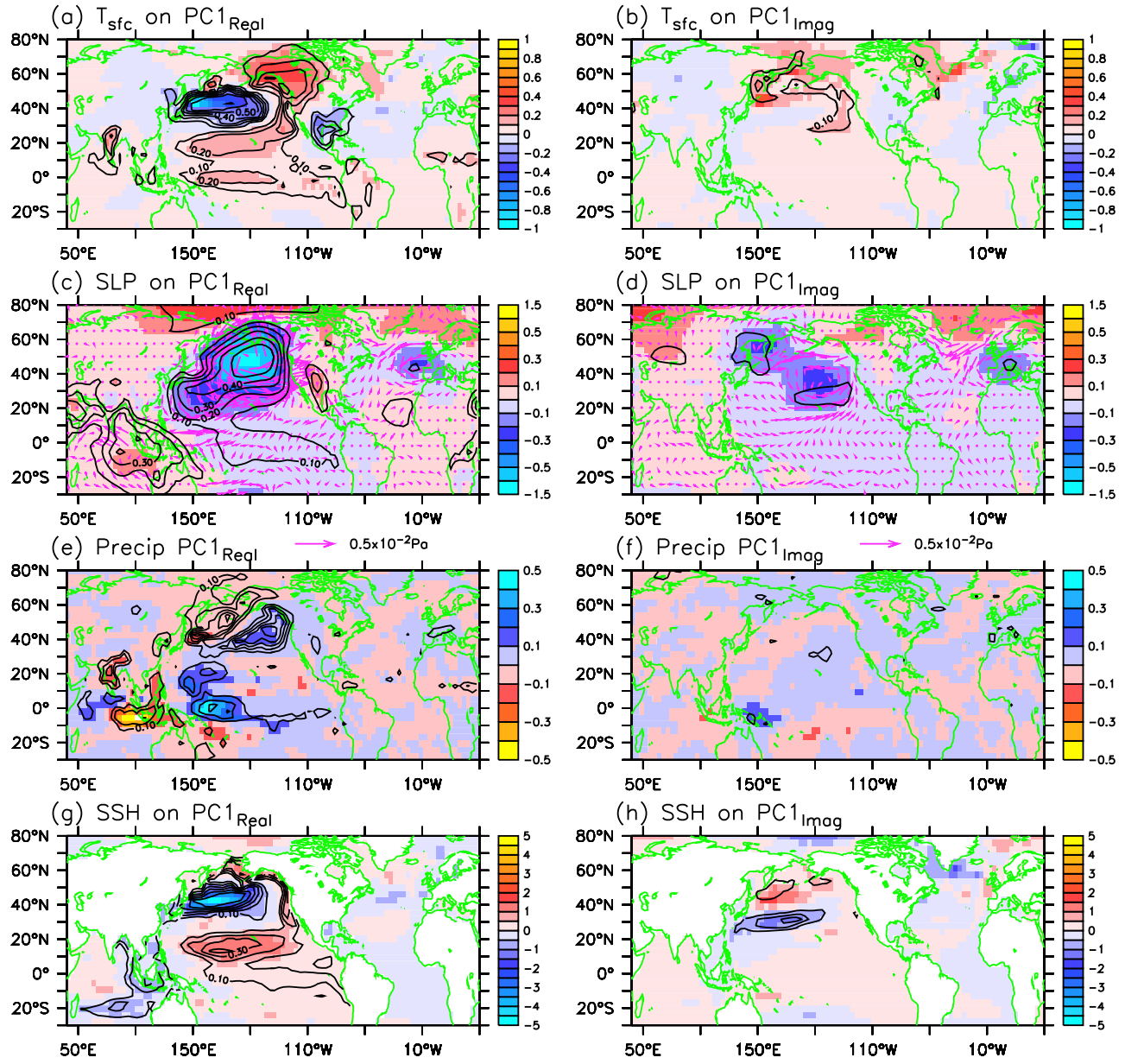

Figure 2. Regression patterns (color) and explained variances (contour) with respect to POP1 (PDV) of (a, b) surface temperature [°C], (c, d) sea level pressure [hPa] and wind stress [Pa], (e, f) precipitation [mm/day] and (g, h) sea surface height [cm] onto the first POP (left) real and (right) imaginary PCs. A 21-year running mean was applied to the annual mean data prior to the regression analysis.

and again positive anomalies in the region 30°–50°N. The corresponding SLP anomaly pattern (Figure 3d) is a dipole pattern with anomalously low pressure centered over southern Greenland and anomalously high pressure in the region 30°–50°N. The associated enhanced wind stress curl south of Greenland (not shown) favors convection there by a spin-up of the subpolar gyre presumably through enhanced salinity advection.

[13] Deep convection is simulated in our coarse-resolution ocean model mostly in the GIN Sea, while the deep convection observed in the Labrador Sea is shifted to the open ocean south of Greenland. We hypothesize that the open ocean convection site is most important for the generation of the multidecadal variability. This would explain the structure of the SLP anomaly pattern (Figure 3d) which goes along with the multidecadal variability. The pattern is not exactly the NAO pattern which is the leading (EOF) mode of SLP variability in KCM, although the regression pattern (Figure 3d) does project on it. As shown by *Park and Latif* [2008], the multidecadal variability in the North Atlantic is strongly linked to the AMOC. Our POP analysis implicitly extracted the AMOC-related multidecadal variability and thus "forces" the SLP anomaly pattern to be consistent with it. The AMV mechanism in KCM is then basically that proposed by *Eden and Jung* [2001], in the sense that low-frequency atmospheric changes drive the North Atlantic overturning circulation.

[14] The SAT and sea level pressure SLP anomalies extend to Eurasia and all the way to the Pacific coast. The SSH anomaly pattern (Figure 3h) with its strong negative

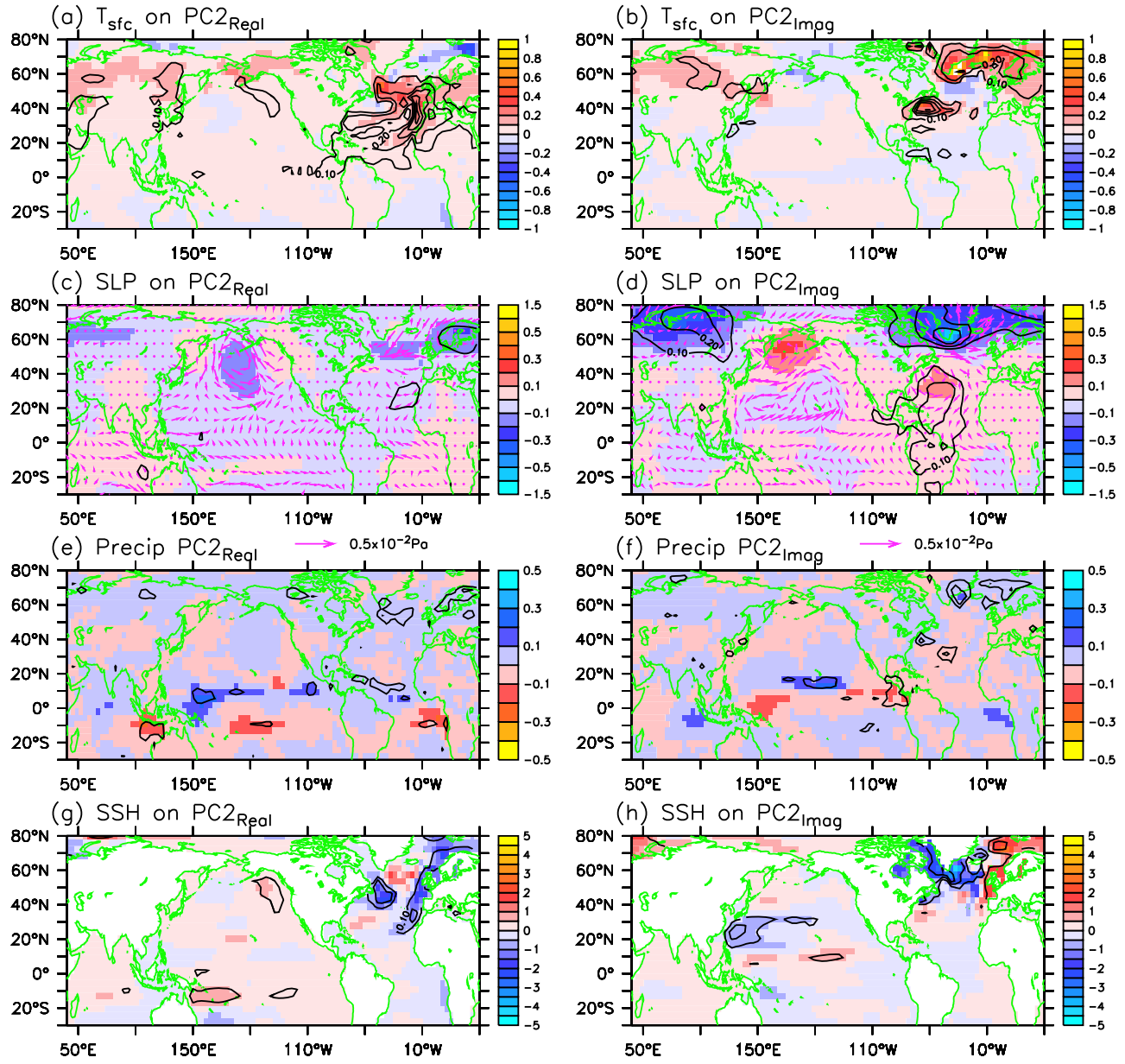

Figure 3. Regression patterns (color) and explained variances (contour) with respect to POP2 (AMV) of (a, b) surface temperature [°C], (c, d) sea level pressure [hPa] and wind stress [Pa], (e, f) precipitation [mm/day] and (g, h) sea surface height [cm] onto the first POP (left) real and (right) imaginary PCs. A 21-year running mean was applied to the annual mean data prior to the regression analysis.

anomalies in the northern North Atlantic reflects a spin-up of the subpolar gyre in response to the intensified westerlies over the North Atlantic (Figure 3d). The associated precipitation pattern is rather patchy. There is enhanced rainfall over the strong warm SAT anomalies in the northern North Atlantic and a teleconnection to the Equatorial Pacific indicating a northward shift of the Intertropical Convergence Zone (ITCZ).

[15] The real part patterns that are shown in Figure 3 (left) display conditions about a quarter of the rotation period later, i.e., after about 15 years. The salient feature is the broad positive SST anomaly covering most of the North Atlantic with explained variances of more than 20% (Figure 3a). As expected from the *Eden and Jung* [2001] mechanism this SST anomaly is a consequence of the AMOC spin-up and enhanced northward heat transport. Indeed, *Park and Latif* [2008] have shown that the SST anomaly pattern is associated with an anomalously strong AMOC. The other regression patterns do not show much of a signal. Precipitation anomalies (Figure 3e) are still seen in the Tropics and the negative SSH anomalies have propagated southward (Figure 3g). Spectra from North Atlantic SLP indices are basically white, indicating no feedback from the ocean to the atmosphere and that, as in the case of PDV, a stochastic scenario applies to AMV.

4. Summary

[16] We have investigated multidecadal sea surface temperature (SST) variability in the North Pacific and North

Atlantic simulated in a millennial scale integration of the Kiel Climate Model. The results indicate that the two leading multidecadal modes, the Pacific decadal variability and Atlantic multidecadal variability are independent phenomena in the model. They have slightly different periods: the main PDV period amounts to about 45 years, while that of AMV to about 60 years. The associated SST pattern is stationary in the case of PDV and non-stationary in the case of AMV. The memory of the two oscillations resides in the subtropical gyre and meridional overturning circulation, respectively. In addition to the multidecadal variability, shorter-term decadal variability is simulated in both oceans, which will be the topic of a forthcoming paper. In the North Pacific, for instance, a quasi-decadal and a bi-decadal mode are simulated by KCM. These also appear to be independent of the variability in the North Atlantic.

[17] **Acknowledgments.** This work is a contribution to the DFG-funded SFB754 (www.sfb754.de) and the Excellence Cluster "The Future Ocean", and has been also supported by the European Union's THOR-project. The model integrations were performed at the Computing Centre of Kiel University and at DKRZ Hamburg.

References

D'Arrigo, R., et al. (2005), Tropical–North Pacific climate linkages over the past four centuries, *J. Clim.*, *18*, 5253–5265, doi:10.1175/JCLI3602.1.

d'Orgeville, M., and W. R. Peltier (2007), On the Pacific Decadal Oscillation and the Atlantic Multidecadal Oscillation: Might they be related?, *Geophys. Res. Lett.*, *34*, L23705, doi:10.1029/2007GL031584.

Delworth, T., S. Manabe, and R. J. Stouffer (1993), Interdecadal variations of the thermohaline circulation in a coupled ocean-atmosphere model, *J. Clim.*, *6*, 1993–2011, doi:10.1175/1520-0442(1993)006<1993:IVOTTC>2.0.CO;2.

Deser, C., A. S. Phillips, and J. W. Hurrell (2004), Pacific interdecadal climate variability: Linkages between the tropics and the North Pacific during boreal winter since 1900, *J. Clim.*, *17*, 3109–3124, doi:10.1175/1520-0442(2004)017<3109:PICVLB>2.0.CO;2.

Dommenget, D., and M. Latif (2008), Generation of hyper climate modes, *Geophys. Res. Lett.*, *35*, L02706, doi:10.1029/2007GL031087.

Eden, C., and T. Jung (2001), North Atlantic interdecadal variability: Oceanic response to the North Atlantic Oscillation (1865–1997), *J. Clim.*, *14*, 676–691, doi:10.1175/1520-0442(2001)014<0676:NAIVOR>2.0.CO;2.

Goldenberg, S. B., C. W. Landsea, A. M. Mestas-Nunez, and W. M. Gray (2001), The recent increase in Atlantic hurricane activity: Causes and implications, *Science*, *293*, 474–479, doi:10.1126/science.1060040.

Gu, D. F., and S. G. H. Philander (1997), Interdecadal climate fluctuations that depend on exchanges between the tropics and extratropics, *Science*, *275*, 805–807, doi:10.1126/science.275.5301.805.

Hasselmann, K. (1988), PIPs and POPs: The reduction of complex dynamical systems using principal interaction and principal oscillation patterns, *J. Geophys. Res.*, *93*, 11,015–11,021, doi:10.1029/JD093iD09p11015.

Knight, J. R., R. J. Allan, C. K. Folland, M. Vellingda, and M. E. Mann (2005), A signature of persistent natural thermohaline circulation cycles in observed climate, *Geophys. Res. Lett.*, *32*, L20708, doi:10.1029/2005GL024233.

Kushnir, Y. (1994), Interdecadal variations in North-Atlantic sea-surface temperature and associated atmospheric conditions, *J. Clim.*, *7*, 141–157, doi:10.1175/1520-0442(1994)007<0141:IVINAS>2.0.CO;2.

Latif, M. (2006), On North Pacific multidecadal climate variability, *J. Clim.*, *19*, 2906–2915, doi:10.1175/JCLI3719.1.

Latif, M., and T. P. Barnett (1994), Causes of decadal climate variability over the North Pacific and North America, *Science*, *266*, 634–637, doi:10.1126/science.266.5185.634.

Latif, M., M. Collins, H. Pohlmann, and N. Keenlyside (2006), A review of predictability studies of Atlantic sector climate on decadal time scales, *J. Clim.*, *19*, 5971–5987, doi:10.1175/JCLI3945.1.

Liu, Z., L. Wu, R. Gallimore, and R. Jacob (2002), Search for the origins of Pacific decadal climate variability, *Geophys. Res. Lett.*, *29*(10), 1404, doi:10.1029/2001GL013735.

Madec, G. (2008), NEMO ocean engine, *Note Pole Model.*, *27*, 1288–1619.

Mantua, N. J., S. R. Hare, Y. Zhang, J. M. Wallace, and R. C. Francis (1997), A Pacific decadal climate oscillation with impacts on salmon, *Bull. Am. Meteorol. Soc.*, *78*, 1069–1079, doi:10.1175/1520-0477(1997)078<1069:APICOW>2.0.CO;2.

Minobe, S., A. Kuwano-Yoshida, N. Komori, S.-P. Xie, and R. J. Small (2008), Influence of the Gulf Stream on the troposphere, *Nature*, *452*, 206–209, doi:10.1038/nature06690.

Park, W., and M. Latif (2008), Multidecadal and multicentennial variability of the meridional overturning circulation, *Geophys. Res. Lett.*, *35*, L22703, doi:10.1029/2008GL035779.

Park, W., N. Keenlyside, M. Latif, A. Ströh, R. Redler, E. Roeckner, and G. Madec (2009), Tropical Pacific climate and its response to global warming in the Kiel Climate Model, *J. Clim.*, *22*, 71–92, doi:10.1175/2008JCLI2261.1.

Roeckner, E., et al. (2003), The atmospheric general circulation model ECHAM5. Part I: Model description, *Rep. 349*, 127 pp., Max Planck Inst. for Meteorol, Hamburg, Germany.

Timmermann, A., M. Latif, R. Voss, and A. Grotzner (1998), Northern Hemispheric interdecadal variability: A coupled air-sea mode, *J. Clim.*, *11*, 1906–1931.

Trenberth, K. E., and J. W. Hurrell (1994), Decadal atmosphere-ocean variations in the Pacific, *Clim. Dyn.*, *9*, 303–319, doi:10.1007/BF00204745.

Valcke, S. (2006), OASIS3 user guide, *PRISM Tech. Rep. 3*, 64 pp., CERFACS, Toulouse, France.

Von Storch, H., T. Bruns, I. Fischer-Bruns, and K. Hasselmann (1988), Principal Oscillation Pattern analysis of the 30- to 60-day oscillation in a general circulation model equatorial troposphere, *J. Geophys. Res.*, *93*, 11,022–11,036, doi:10.1029/JD093iD09p11022.

Zhang, R., and T. L. Delworth (2006), Impact of Atlantic multidecadal oscillations on India/Sahel rainfall and Atlantic hurricanes, *Geophys. Res. Lett.*, *33*, L17712, doi:10.1029/2006GL026267.

Zhang, R., and T. L. Delworth (2007), Impact of the Atlantic Multidecadal Oscillation on North Pacific climate variability, *Geophys. Res. Lett.*, *34*, L23708, doi:10.1029/2007GL031601.

M. Latif and W. Park, Leibniz-Institut für Meereswissenschaften an der Universität Kiel (IFM-GEOMAR), Duesternbrooker Weg 20, D-24105 Kiel, Germany. (wpark@ifm-geomar.de)